5th SASTech
Iran |Mashhad
May 12 - 17 | 2011
5th Symposium on Advances in Science & Technol

Effect of geometrical order on the optical properties of metal nanoparticles

Soheila Moghadam, Soheilamoghadam@gmail.com
Mahmoud Aleshams, m_aleshams@yahoo.com
Department of Electrical Engineering, Bushehr Branch,
Islamic Azad University, Bushehr, Iran
Paper Reference Number: 20
Name of the Presenter: Aoheila Moghadam

Abstract

In this paper, we study the theoretical computational of the optical properties of collections of metal nanoparticles with electromagnetic interparticle interaction. The linear optical properties of MNPs are determined by localized surface Plasmon resonance. The LSPR for a MNP depends on substance, size, shape and surroundings. There are three classes of plasmons, depending on the geometry of the metal under study. Second-order generation is the nonlinear properties of MNPs. It has been used to study ultrafast electron dynamics in MNPs by second order autocorrelation, or local electric-field effects like surface enhanced Raman scattering, but has been rarely considered on its own merits. Interaction between multiple particles with defined geometrical arrangements are considered.
Key words: Nanoparticle, Surface Plasmon, Mie theory

1. Introduction

Small bits of metal have strong optical resonances in the visible and near-visible region of the photonic spectrum. This size range (from one to one hundred nanometers) is becoming known popularly as the nanoscale, and these small-but-not-too-small bits we refer to as metal nanoparticles (MNPs). In plainer terms, MNPs light up at various colors.

In 1908 Gustav Mie published analytical expressions for the electromagnetic surface modes of small metal spheres, demonstrating the optical resonances and giving Faraday's idea firm theoretical footing[13]. The intervening century of research has established that these "Mie resonances" are due to a collective electronic behavior, known as the localized surface Plasmon resonance (LSPR), which depends on the substance, size, shape, and surroundings of the nanoparticle [2,9].

The surroundings may be thought of as comprising two categories. The primary meaning is the local dielectric environment of the nanoparticle. As used in this work, it also includes the possibility of electromagnetic interactions with nearby metal particles or surfaces. Interactions

between multiple particles with well-defined geometrical arrangements are of particular interest in this work. Size effects are somewhat complex, but the most typical occurrence is that the LSPR will redshift with increasing size.
The LSPR depends strongly on shape. A sphere will have a single resonance, since it looks the same from all directions. In contrast, a general ellipsoid that has three unequal axes will have three different (but not independent) LSPR modes; that is, it will have a different color viewed from different directions. Fortunately, there are convenient mathematical formulations for "nice" shapes like ellipsoids. Unfortunately, even for ellipsoids the analysis is very complex[2], and convenient formulas for some more complex shapes have not been found.
The linear optical properties of MNPs are determined by the localized surface plasmon resonance (LSPR). A Plasmon is a collective oscillation of electrons in a metal. There are three classes of Plasmons, depending on the geometry of the metal under study.
A surface plasmon is a collective longitudinal oscillation of electrons that occurs at a boundary between a metal and a dielectric. The conduction electrons involved are all at the surface of the metal. A related excitation sometimes confused with the surface plasmon is the surface Plasmon polariton. The difference is that the polariton excitation is coupled with photons, whereas a plasmon strictly speaking is not. This difference is clarified in the nanoparticle case by the different dispersion of surface-plasmon-polaritons and "free" surface plasmons for larger nanoparticle sizes[9].
section 2 introduces theoretical computations of the optical response of MNPs.

2.Computational Modeling

We have advanced the state of the art in the computation of the optical properties of arrays of metal nanoparticles, by taking account of specific excitation and detection geometries other than traditional normal incidence extinction within a coupled-dipole formalism.
Metal nanoparticles are already finding use through their linear optical properties in biochemical sensing applications [6,12].
Gustav Mie's now century-old classical theory describing the optical response of a metal sphere embedded in a dielectric has been remarkably successful despite its limited scope[9,13]. The LSPR resonances of metal nanoparticles are now known to depend upon the shape and arrangement as well as the size and dielectric environment of the particles. Here, we present computations of the optical properties of collections of metal nanoparticles with electromagnetic interparticle interaction. Along the way, we give a rough sketch of the theoretical basis for the optical properties of metal nanoparticles.
Numerical simulations of the optical properties of metal nanoparticles are desirable for a number of reasons. First, when done by computer they represent perhaps the fastest way to compare experimental results with theoretical models. Second, when the models have been shown to match experimental results, they can be used in a predictive manner to guide the experimenter's craft. Third, there exist only a handful of cases (spheres, ob-late/prolate ellipsoids) that yield analytical solutions to Maxwell's equations, and even then one is often restricted to particles much smaller than the wavelength of light (i.e. quasistatic approximation)[2]. For larger sizes, other shapes (such as general ellipsoids, or cubes[4]), and especially for large sizes of other shapes [1], the mathematical expressions can be rather frightening, and in general numerical simulation is necessary. We note in passing the existence of several numerical methods used to calculate the optical response of nanoparticle systems, particularly with nonspheroidal shapes, which will not be discussed in detail: T-

matrix methods [14], finite-difference time-domain calculations (FDTD) [11], discrete dipole approximation (DDA) [7], multiple multipole approxima-tion (MMA) [15], and conjugate gradient fast Fourier transform (CG-FFT) [10]. We will focus on the coupled dipole approximation (CDA) [8], as it is perhaps the most convenient for calculating the response of arrays of particles especially particles like spheroids, whose polarizability may be put in a tractable form.

The nonlinear characteristics of MNPs are not nearly as well-known as the linear properties. We limit the discussion here to second-order nonlin-earities. In particular, second harmonic generation (SHG) has been used frequently to study ultrafast electron dynamics in MNPs by second-order autocorrelation, or local electric-field effects like surface-enhanced Raman scattering (SERS), but has been rarely considered on its own merits.

The primary difficulty with studying SHG in metal nanoparticle arrays is the well-known fact that symmetry forbids the generation of even harmonics by electric dipole sources in the forward and backward directions. Most researchers have only considered the traditional normal-extinction geometry in which excitation and detection are both perpendicular to the sample; in such an arrangement, second-harmonic light cannot be observed from symmetric particles. For second-order autocorrelation measurements, there-fore, it has been necessary to use asymmetric particle shapes like triangles.

3.Coupled Dipole Approximation

The Coupled Dipole Approximation(CDA) models the dipolar (lowest-order) optical response of arrays of individual nanoparticles, without including higher-order multipoles. The dipole moment induced in a single particle by a local electric field is given by the equation (SI units)

$$\vec{p}_i = \varepsilon_0 \alpha_i \vec{E}_{loc}(\vec{r}_i) \quad (1)$$

$\vec{p}_i$ is the induced dipole moment, α_i is the polarizability of the particle cen-tered at $\vec{r}_i$, $\vec{E}_{loc}$ is the local electric field, and $\varepsilon_0$is the permittivity of free space. As an example, for spheres in the quasistatic approximation (QSA) (radius a <<λ), the polarizability takes the form

$$\alpha = 3V \frac{\varepsilon - \varepsilon_m}{\varepsilon + 2\varepsilon_m} \quad (2)$$

Where $V = \frac{4\pi}{3} a^3$ is the sphere volume, ε is the dielectric function of the particle and ε_m is the dielectric function of the surrounding medium. It is immediately seen from Eq. 2. that a resonance in the polarizability will occur when the following condition is satisfied:

$$\varepsilon = -2\varepsilon_m \quad (3)$$

Other forms of the polarizability, including the modified long-wavelength approximation (MLWA) and a dipolar approximation from Mie theory, will be discussed below.

The local field arises from two sources, appearing as two terms. The first term is the incident light, The second term is the superposition of the retarded fields from each of the other N-1 radiating dipoles in the array. Combining these terms, we have for the local field.

$$\vec{E}_{inc,i} = \alpha^{-1}\vec{p}_i + \sum_{j \neq i} A_{ij}\vec{p}_j \quad (4)$$

in which the A_{ij} are 3 x 3 matrices representing the interaction of two particles i and j. The optical properties may then be calculated from this dipole array; for example, the unitless scattering efficiencies follow.

$$Q_{sca} = \frac{k^4}{6\pi^2 a^2 \varepsilon_0^2 |\vec{E}_{inc}|^2} \sum_{i=1}^{N} \left| \vec{E}_{inc}^{*} \cdot \vec{p}_i \right|^2 \quad (5)$$

Fortunately, one is not limited to calculating extinction efficiencies and cross- sections once the dipole array is found. Specifically, the time-averaged power P radiated per unit solid angle

Ω by an oscillating dipole moment $\vec{p}$ the direction $\hat{n}$ to the far field is [34].

$$\frac{dP}{d\Omega} = \frac{c^2 z_0}{32\pi^2} k^4 |(\hat{n} \times \vec{p}\,) \times \hat{n}|^2 \quad (6)$$

in which c is the speed of light and Z_0 is the impedance of free space. Eq.6 may be integrated over a given solid angle to yield the power radiated into that solid angle,

$$P = \frac{c^2 z_0}{32\pi^2} k^4 \iint |(\hat{n} \times \vec{p}\,) \times \hat{n}|^2 \sin\theta \, d\theta d\varphi \quad (7)$$

where the double integral runs over the desired limits for polar θ and azimuth φ angles. The integration limits are determined by the angular size and position of the light collection device to be used in the experiment, e.g. a microscope objective lens. We may solve the double integral numerically to find the power.

The optical properties of one-dimensional chains and two-dimensional arrays of Ag nanospheres with were studied with the CDA and the T-matrix method, which is an exact calculation based on Mie theory [19]. It was found for 1-D chains that multi-polar effects become especially important when particles approach closely; in particular, the CDA is inadequate when the gap between neighboring particles is on the order of half the particle radius. For 2-D arrays the CDA captures the most important array effects. For Ag spheres with radius 30 nm, as the spacing is decreased from large values to 75 nm (so spacing/diameter = 1.25) the LSPR blueshifts; as the particles approach even more closely the LSPR redshifts slightly. In addition, the LSPR spectral width narrows slightly from large spacing down to 180 nm (spacing/diameter = 3) and then broadens considera-bly at still smaller spacings. This behavior results from the interaction of the retarded dipole sums with the particle plasmon properties.

It was pointed out that multipole resonances, which are important for large spheres, are suppressed in large ellipsoids with high aspect ratios. Thus, the quasistatic approxi-mation may be useful for ellipsoids even when it fails for spheres of the same volume.

The optical properties of two interacting metal nanodisks were studied by experiment and computation for Au and Ag [5,16]. The experimental data were fit to a coupled-dipole model with reasonable agreement. For light polarized along the nanoparticle-pair axis, Coulomb attraction between the positive end of one dipole and the negative end of the other reduces the interaction energy, redshifting the LSPR as the particles approach. For light polarized perpendicular to the pair axis, repulsion between the positive and negative sides of neighboring particles increases the interaction energy, blueshifting the LSPR as the particles approach.

Narrow LSPR lineshapes (~1 nm) were found for one-dimensional chains of Ag nanospheres [20] with large spacing. The narrowing is due to interference effects, imply-ing that an infinite chain produces the narrowest spectra. For 2-D arrays, the narrowing is much less pronounced.

We now show a broad-brush outline of the algorithm used, and give several recommendations for these computations. The polarizability is wavelength-dependent through the complex dielectric function, so it is solved first. The dipole array is used directly to compute the extinction properties.

4.Polarizability Forms

In Section 2 we noted the quasistatic form of the polarizability for spheres in the CDA. There are several other versions of the polarizability that may be used within the basic formalism, depending on particle shape and the desired model. We now give an overview of these expressions. The QSA is a severe limitation when calculating the optical properties of

spheres. Specifically, it ignores any spectral size-dependence of the resonance (other than scaling with volume). For sufficiently large particles it is necessary to adjust the particle polarizabilities to take into account two factors: 1) radiative damping, i.e. the effect of the reradiated field on the particle plasmon behavior, and 2) dynamic depolarization, caused by the finite ratio of particle size to wavelength (so that the QSA does not strictly hold). The resulting modifications to the polarizability constitute the modified long wavelength approximation (MLWA). First we write a more general form of the polarizability:

$$\alpha = 3V\frac{\varepsilon-\varepsilon_m}{\varepsilon_m+L(\varepsilon-\varepsilon_m)F} \quad (8)$$

Where $\varepsilon_m$is the dielectric function of the surrounding medium, L is a shape factor $=\frac{1}{3}$ for spheres, and within the QSA F=1, To apply the MLWA we set

$$F_{MLWA} = 1-(ka)^2-\frac{2}{3}i(ka)^3 \quad (9)$$

Here a is the sphere radius (for ellipsoids it should be replaced with the semi-axis of interest). The second term corresponds to dynamic depolarization, the third to radiative damping [17].
Mie Theory. Mie's treatment of spheres leads to expressions for scattering coefficients that may be used to calculate measurable quantities like optical efficiencies and cross-sections for single isolated particles. However, these coefficients may themselves be incorporated into the coupled-dipole formalism; that is, an effective electric dipole polarizability may be calculated from the first-order scattering coefficient, as demon-strated by Doyle [3].
Comparison of Mie/Quasistatic/MLWA. We may examine the range of applicability of the Mie-dipole approximation by comparing with the exact Mie theory for spheres. Fig.1 shows that for Ag spheres in vacuum, the Mie-dipole approximation closely follows the exact Mie extinction efficiency up to at least particle radius 50 nm. The exact Mie results indicate that at this size, the dipolar mode still dominates the small quadrupolar shoulder that occurs at higher energies. For particles of 100 nm radius (not shown), the short-wavelength shoulder develops into the strongest peak; the dipole no longer dominates and this approximation is no longer valid.

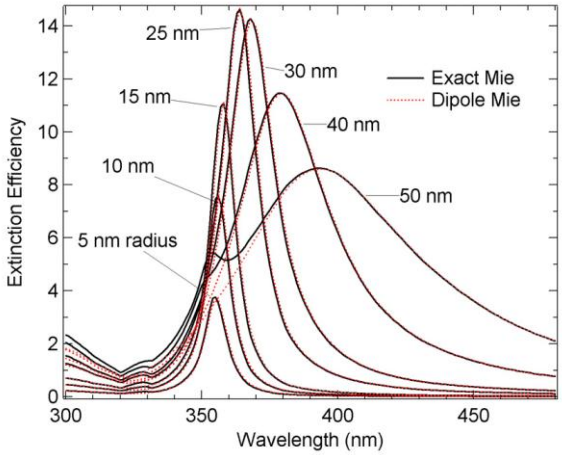

Fig.1. Comparison of Mie dipole approximation with exact Mie theory.

Fig.2 demonstrates the size dependence of the QSA and MLWA compared with the dipolar Mie model for Ag spheres. Clearly, the quasistatic spectrum is unchanged with size, as expected from Eq.2. For 5 nm radius, the correspondence with Mie theory is exact. As size increases, the QSA becomes progressively worse. (Somewhat ironically, the QSA works best

where it works worst, because 5 nm radius in Ag is approximately where the real part of the dielectric function begins to depend strongly on particle size [10]). The MLWA is a considerable improvement at intermediate sizes, as the increased radiation damping with size is reflected in decreased amplitudes and the dynamic depolarization is seen in the redshift. However, at 40 nm radius, the redshift is exaggerated by 20 nm, and for 50 nm radius by 40 nm. In light of the fact that the Mie di-pole expressions may be programmed fairly readily (provided one is willing to wrangle Riccati-Bessel functions) and do not appear to pose a significantly increased computa-tional burden relative to the MLWA, it seems prudent to base any extinction calculations for spheres on the Mie-dipole formalism. We should note that the MLWA appears to be more useful for ellipsoids [8], for which exact computation schemes are much rarer, though they do exist[20].

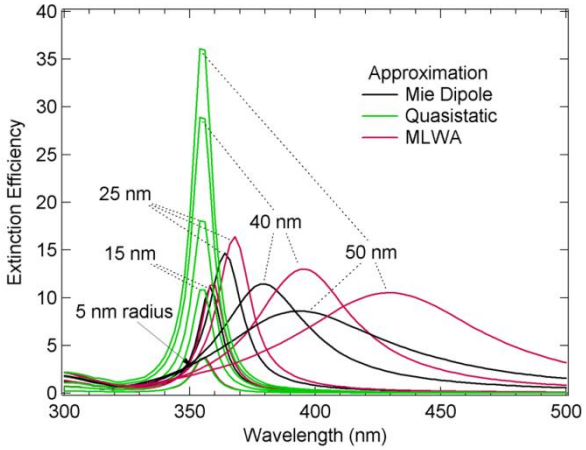

Fig.2. Comparison of Mie dipole approximation, QSA, and MLWA for various particle sizes.

Ellipsoids. The general form of the polarizability for an ellipsoid in the quasistatic approximation with semiaxes $a \gg b \gg c$ is as follows:

$$\alpha = V \frac{\varepsilon - \varepsilon_m}{\varepsilon_m + L_i(\varepsilon - \varepsilon_m)} \tag{10}$$

The shape factors L_i for the three possible axes obey the sum rule $\sum_{i=1}^{3} L_i = 1$.

For spheres the shape factors all collapse to $L_i = \frac{1}{3}$, by which we arrive at Eq. 2. For oblate and prolate spheroids, analytical expressions of the shape factors may be found. We list only the expression for an oblate spheroid, as it is a good approximation to a lithographically prepared disk.

$$L_1 = \frac{g(e)}{2e^2}\left[\frac{\pi}{2} - \tan^{-1} g(e)\right] - \frac{g(e)^2}{2} \tag{11}$$

$$e^2 = 1 - \frac{c^2}{b^2}$$

$$g(e) = \sqrt{\frac{1-e^2}{e^2}} = \sqrt{\frac{c^2}{a^2 - c^2}}$$

Here e is the eccentricity of the spheroid, where the limiting values are a disk (1) and a sphere (0). For the oblate spheroid, $L_1 = L_2$.

The expressions for the shape factors of general ellipsoids are in integral form, as follows (here i=a, b, c);

$$L_i = \frac{abc}{2}\int_0^\infty \frac{dq}{(i^2+q)\sqrt{(a^2+q)(b^2+q)(c^2+q)}} \quad (12)$$

The shape factor integral calculations are extraordinarily useful for calculating the linear optical properties of isolated metal nanoparticles, again within the quasistatic approximation. Combined with the dielectric function of the material, they can predict resonance peak positions for all three axes.

In Fig.3, we show the effects of increasing particle number for 45° dark-field incidence with s-polarized light. As an aid to the eye, the scattering efficiencies have been multiplied by particle number for comparison with the power graph. Again we see that the detector response captures certain interference effects not present in the scattering efficiency.

At normal incidence, all particles are excited in phase; one might expect that the co-herence properties dictate that in the forward-scattered direction, the spectrum will not be altered much by varying detector size. However, for a dark-field illumination scheme, the situation is evidently quite different, and the effects of detector geometry should be taken into account in order to accurately compare theory and measurement.

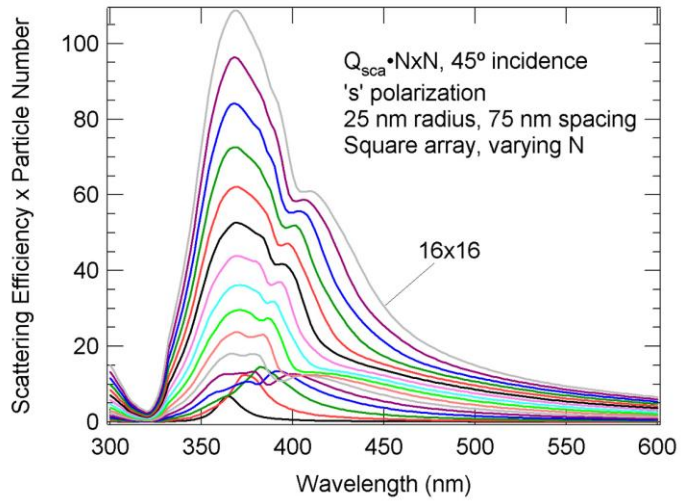

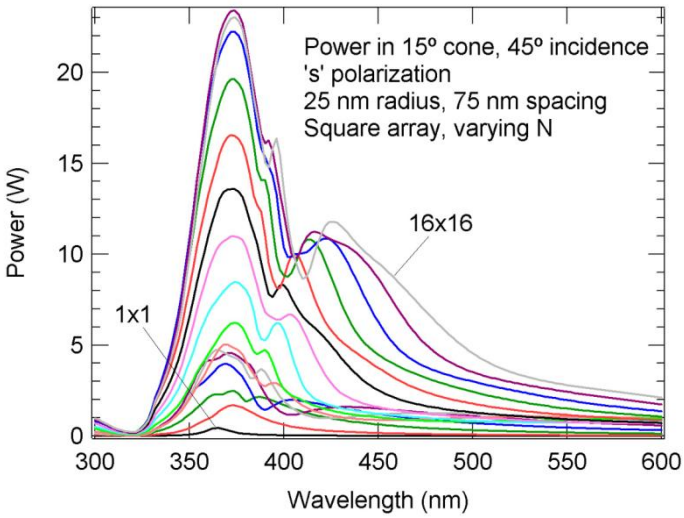

Fig.3. Comparison of a) scattering efficiencies and b) integrated power for varying particle number at 45° incidence. Scattering efficiencies are multiplied by the number of particles in the array as a visual aid.

5. Conclusions

The linear optical properties of MNPs (those properties that are independent of the irradiance) are determined by LSPR.The LSPR for a given MNP depends on the Substance, Size, Shape , Surroundings. A sphere will have a single resonance, since it looks the same from all directions. In contrast, a general ellipsoid that has three unequal axes will have three different (but not independent) LSPR modes; that is, it will have a different color viewed from different directions. The simplest geometric approximation to these particle shapes is the general ellipsoid (semiaxes $a \gg b \gg c$). There has not been a method for examining the second-order nonlinear optical properties of MNP arrays whose linear optical properties are relatively well-known and easily calculable.

We have advanced the state-of-the-art in the computation of the optical properties of arrays of metal nanoparticles, by taking account of specific excitation and detection geometries other than traditional normal-incidence extinction within a coupled-dipole formalism.

References

Asano ,S. and Yamamoto ,G., (1975). Applied Optics 14, 29.

Bohren, C. F. and Huffman,D. R. (1983).*Absorption and Scattering of Light by Small Particles*. Wiley-Interscience, New York.

Doyle,W. T. (1989). Physical Review B 39, 9852.

Fuchs,R. (1975). Physical Review B 11, 1732.

Gunnarsson,L. T. (2005).Journal of Physical Chemistry B 109, 1079.

Haes,A. J., Haynes,C. L., McFarland,A. D., (2005). MRS Bulletin 30, 368

Jensen,T., Kelly,L., Lazarides,A. and Schatz,G. C. (1999). Journal of Cluster Science 10, 295.

Kelly,K. L., Coronado,E., Zhao, L. L. and G. C. Schatz, (2003). Journal of Physical Chemistry B 107, 668.

Kreibig U. and Vollmer,M. (1995).*Optical Properties of Metal Clusters*. Springer Series in Materials Science, Vol. 25, Springer Verlag, Berlin-Heidelberg.

Lazarides ,A. A. and Schatz,G. C. (2000). Journal of Chemical Physics 112, 2987.

Maier,S. A., Kik, P. G. and Atwater,H. A. (2003). Physical Review B 67.

McFarland, A. D. and Van Duyne, R. P. (2003). Nano Letters 3, 1057.

Mie,G. Annalen der (1908).Physik 25, 377.

Mishchenko,M. I., Travis,L. D. and Mackowski, D. W(1996). Journal of Quantitative Spectroscopy & Radiative Transfer 55, 535.

Moreno,E., (2002).Journal of the Optical Society of America A 19, 101.

Rechberger, W., Hohenau,A. (2003). Optics Communications 220, 137.

Soller B. J. and Hall,D. G. (2002). Journal of the Optical Society of America B 19, 1195.

Voshchinnikov N. V. and Farafonov,V. G. (1993). Astrophysics and Space Science 204, 19.

Zhao,L. L., Kelly,K. L. and Schatz,G. C. (2003). Journal of Physical Chemistry B 107, 7343.

Zou,S. L., Janel, N. and Schatz, G. C. (2004). Journal of Chemical Physics 120, 10871.